Journal of Metals, Materials and Minerals, 34(2), 1969, 2024

Influence of annealing times for W films on the structure and electrochromic properties of anodized WO_3 films

Watcharaporn THONGJOON[1], Kamon AIEMPANAKIT [1,*], Montri AIEMPANAKIT[2], and Chantana AIEMPANAKIT[3]

[1] *Department of Physics, Faculty of Science and Technology, Thammasat University, Pathumthani, 12121, Thailand*
[2] *Department of Physics, Faculty of Science, Silpakorn University, Nakhon Pathom, 73000, Thailand*
[3] *Division of Physics, Faculty of Science and Technology, Rajamangala University of Technology Thanyaburi, Pathumthani, 12110, Thailand*

***Corresponding author e-mail**: akamon@staff.tu.ac.th

Received date:
18 February 2024
Revised date
13 March 2024
Accepted date:
16 April 2024

Keywords:
WO_3;
Annealing;
Sputtering;
Anodization;
Electrochromic properties

Abstract

WO_3 films were prepared from annealed W films by anodization and annealing at 450°C for 1 h. The sputtered W films were annealed before anodization at different times for 0.5 h to 2 h, followed by immediate removal from the furnace (quenching) or slow cooling (cool-down). The WO_3 films exhibited a different preferred orientation between the (200) and (222) planes. The morphological structure of the WO_3 films depended on the annealing time and cooling features of the W films. The WO_3 films for the cool-down condition had smaller grains and more pores than the quenching condition. The WO_3 films prepared from annealed W for 1.5 h with cool-down showed maximum transmittance change of 48.20% with the diffusion coefficient of 3.533×10^{-7} $cm^2 \cdot s^{-1}$. The quenching condition can be improved durability of WO_3 films. Therefore, annealing time and cooling conditions can be used to design film properties that are suitable for the electrochromic application.

1. Introduction

The performance of an electrochromic glass depends on the ability of the electrochromic material. Popular electrochromic materials are the metal oxides of tungsten [1], molybdenum [2], titanium [3], vanadium [4], and nickel [5]. These metal oxides have optical properties that allow light to pass through in visible light, making them transparent. Optical changes in electrochromic properties depend not only on the material type but also on the particle size [6], shape [7], and surface area of the structure [8]. The smaller or more porous structure has better electrochromic properties. Tungsten oxide (WO_3) films are electrochromic materials that have received much attention, because in the as-deposited state, they are colorless and highly transparent; when stimulated (colored state) with voltage they will change to dark blue [9]. This is caused by the insertion of electrons and ions, resulting in changing the oxidation number of W from 6^+ to 5^+. In addition, WO_3 is a cheap, stable material with high coloration efficiency.

The preparation of WO_3 films for electrochromic layers can be done by several methods, such as pulsed laser deposition [10], sputtering [1,6,11,12,17,30], sol-gel [15], anodization [8,9,16,18-20], etc. Each method gives different film results depending on various variables in film preparation. Shi *et al*. [11] prepared WO_3 films by direct current (DC), radio frequency (RF), and pulsed radio frequency (PRF) magnetron sputtering to compare electrochromic properties. The WO_3 films prepared by PRF magnetron sputtering showed a porous morphology compared to WO_3 films obtained by other deposit approaches. When calculating the optical contrast in visible light and near-infrared, the values were equal to 93.6% and 90%, respectively. Zhang *et al.* [12] prepared W films on indium-doped tin oxide (ITO) glass by DC magnetron sputtering. The W films with a thickness of 0.8 μm were anodized. The results showed that the W films before anodization had an amorphous structure and opaque physical characteristics. When the W films were anodized, they changed to WO_3 films with a more transparent physical appearance and a porous morphology. WO_3 films exhibited a coloration efficiency of 58 $cm^2 \cdot C^{-1}$ and took 8 s to reach a colored state.

The structure of WO_3 films affects their electrochromic properties. Ashrit *et al*. [13] reported that the nanocrystalline structure of WO_3 films showed good electrochromic properties in the near-infrared but low efficiency in visible light. On the other hand, its polycrystalline and amorphous structure gives it good performance in visible light. In the same way, Zhang *et al*. [14] study electrochromic properties from the effects of structural differences between the amorphous, crystalline, and composite structures of WO_3. The composite structure of WO_3 films exhibited excellent electrochromic performance with high optical contrast and high coloring efficiency are 70.6% and 53.6 $cm^2 \cdot C^{-1}$, respectively, at a wavelength of 633 nm. Moreover, Purushothaman *et al*. [15] prepared WO_3 films using the sol-gel method. The results indicated that the WO_3 films showed an amorphous

structure and a smooth surface. The WO_3 films exhibited a change in optical transmission of 55.37% at a wavelength of 550 nm. It can be seen that the structure is an essential factor in electrochromic properties. Therefore, structural improvements are necessary.

The electrochromic properties of WO_3 films were improved by creating nanostructures. The anodizing method is one of several methods chosen because it is simple, convenient, and low-cost. There are many factors affecting the improvement of the nanostructure of the WO_3 films, such as electrolyte concentration [16], anodizing time [17], anodizing temperature [18], annealing temperature [19], and voltage anodizing [20], etc. In this research, the researcher is interested in the nanostructured WO_3 films prepared from W films by the sputtering and anodization processes. We focused on the effect of annealing time for the W films on nanostructured WO_3 films and their electrochromic properties.

2. Experimental details

The fluorine-doped tin oxide (FTO) glass substrate (3 cm × 1 cm) was cleaned with acetone, methanol, and deionized water for 15 min each, respectively. The W films were deposited on the cleaned FTO glass by DC magnetron sputtering using a high purity (99.995%) W target disk (2-in diameter and 0.25-in thick, Kurt J. Lesker). The target–substrate distance was approximately 80 mm. The chamber was evacuated to a base pressure through diffusion and rotary pumps at approximately 5×10^{-5} mbar. A constant flow rate of purified argon (Ar) 99.999% at 15 standard cubic centimeter per minute (sccm) was controlled using a mass flow controller with a pressure of approximately 1.9×10^{-3} mbar during the sputtering of the W films. Before deposition, the W target was pre-sputtered in an argon atmosphere for 3 min to remove oxide on the target surface. The sputtering power was kept at 150 W for all samples. The thickness of the W films was approximately 277 nm. The W films were annealed at 250°C in the air for different annealing times for 0.5 h to 2 h and separated into two groups: (1) immediately removed from the furnace (quenching) and (2) slow cooling (cool-down), as shown in Table 1. The annealed W films were structurally improved by anodization in an electrolyte solution prepared by mixing ethylene glycol and 0.6 wt% ammonium fluoride (NH_4F) solution. After that, the anodized films were annealed at 450°C for 1 h. The crystal structure of the WO_3 films was studied by X-ray diffraction (XRD) with Cu Kα radiation at 1.54184 Å (Bruker, D2- PHASER). The morphological structure of the WO_3 films was analyzed by field emission scanning electron microscopy (FE-SEM, TESCAN MIRA-3, Czech Republic), while UV-Vis spectrophotometry (G10S UV-Vis, Thermo Scientific)was used to measure the transmittance spectra of the as-deposited, colored, and bleached states of WO_3 films in a wavelength range from 200 nm to 1,000 nm. The coloration efficiency of the WO_3 films was examined by cyclic voltammetry (CV) with silver/silver chloride (Ag/AgCl) as a reference electrode and platinum (Pt) foil as a counter electrode in a 0.1 M sulfuric acid (H_2SO_4) solution with a scan rate of 100 $mV \cdot s^{-1}$ and applying voltages of –1.5 V to +1.5 V.

3. Results and discussion

The sputtered W films were annealed for improved structure with different times for 0.5 h to 2 h, and the annealed W films were quenched and slowly cooled down before anodization. Figure 1(a-d) shows the morphology of WO_3 films in the quenching condition. The results exhibited that the grain size of WO_3 was larger than in the cool-down condition, as shown in Figures 1(e-h). The different annealing times directly affected the morphology of WO_3. Generally, annealing and slowly cooling down causes the films to become more aggregation of grains, the grain size grows, and oxides can form on the surface and deeper in the films. For the quenching process, the films are immediately exposed to cool outside air. The film's surface is then exposed to large amounts of oxygen, creating additional oxides on the surface that are different from slowly cooling down. In this work, it was found that the structure of WO_3 films prepared under cool-down conditions showed small grain sizes and high porosity. Considering the quenching condition, the WO_3 films became denser, especially in the annealing time condition of 1 h to 1.5 h, which may be due to the dense oxide layer on the W film's surface. Moreover, the annealing at different times showed apparent differences in grain and surface texture of WO_3 films, with the Cd-1 condition showing the finest grains. Table 2 shows the crystallite size, significantly related to the microstrain. The microstrain can be calculated using Equation (1) [21]. The more significant grain boundaries could result from the microstrain being decreased.

$$\beta \cos\theta = \frac{\lambda}{D} + \varepsilon \sin\theta \quad (1)$$

where β is the full width at half maximum (FWHM) of the diffraction peak measured in radians, θ is the diffraction angle, λ is X-ray wavelength, D is crystallite size, and ε is the effective lattice strain.

Table 1. Conditions for annealing of W films.

Annealing time (h)	Conditions of annealing	
	Quenching	Cool-down
0.5	Q-0.5	Cd-0.5
1	Q-1	Cd-1
1.5	Q-1.5	Cd-1.5
2	Q-2	Cd-2

Table 2. The crystallite size and microstrain of the WO_3 films.

Sample	Crystallite size (nm)	Microstrain (10^{-3})
Q-0.5	39.43	1.04
Cd-1	28.25	1.31

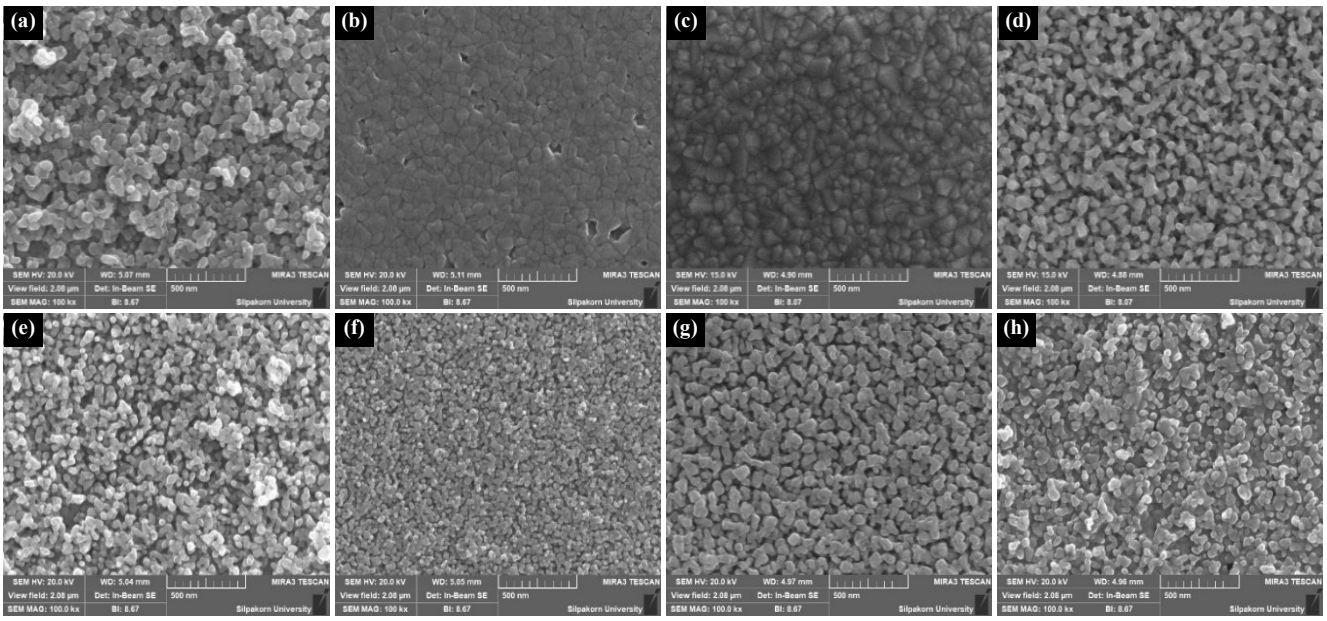

Figure 1. FE-SEM images of WO_3 films anodized from annealed W films at different annealing times of (a) Q-0.5, (b) Q-1, (c) Q-1.5, (d) Q-2, (e) Cd-0.5, (f) Cd-1, (g) Cd-1.5, and (h) Cd-2.

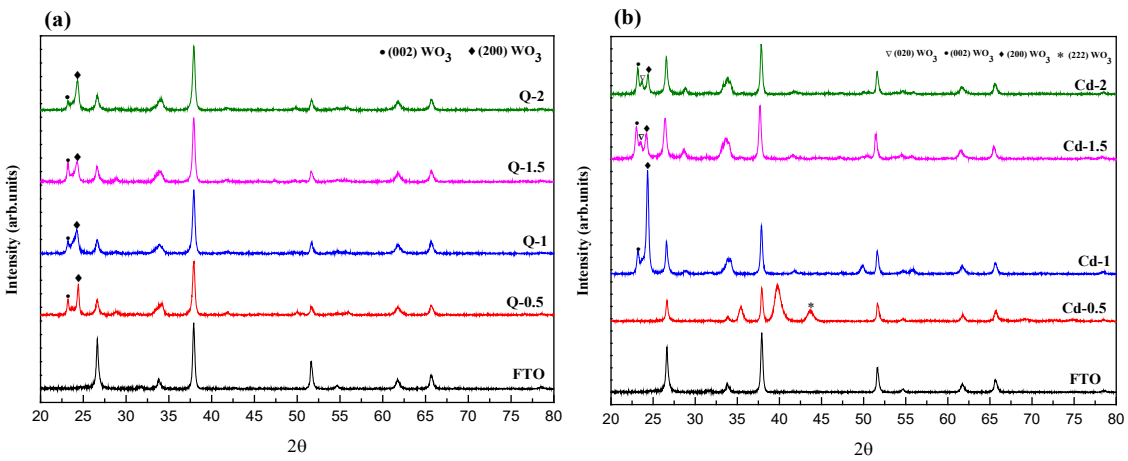

Figure 2. X-ray diffraction of WO_3 films anodized from annealed W films at different annealing times (a) quenching and (b) cool-down.

The results are consistent with the research of Akgul *et al*. [21], which prepared copper oxide films at different temperatures, resulting in different morphologies, and Pandurangarao *et al*. [22], in which WO_3 films were prepared at various substrate temperatures. Crystallite size is induced to vary with temperature

Figure 2 shows the X-ray diffraction analysis of WO_3 films. The results showed that WO_3 films treated with different annealing times appear with (020) (002) (200) and (222) peaks corresponding to 23.30°, 23.81°, 24.45°, and 42.08°, respectively, which are consistent with the monoclinic structure (JCPDS PDF no. 00-043-1035) [23]. The different structure arrangement resulted from the W films treated with different annealing when the temperature was decreased slowly; the cool-down WO_3 films exhibited a better-organized crystal structure. In addition, the crystallite size affects electrochromic properties [24]. This result corresponds to the report by Madhuri *et al*. [25]. Morphology and crystal structure are important factors affecting electrochromic properties [26]. The WO_3 films with many grains and small grains showed better optical properties than WO_3 films with large grain sizes [27]. Meanwhile, WO_3 films with high crystallinity also degrade slowly [28]. The crystallite size can be calculated using the Scherrer equation as shown in Equation (2).

$$D = \frac{K\lambda}{\beta cos\theta} \quad (2)$$

where D is crystallite size, K is the shape factor (0.9), λ is the wavelength of the X-ray, β is full width at half maximum intensity, and θ the diffraction angle.

Analysis of electrochromic properties using the CV technique is shown in Figure 3. They can indicate the coloration performance, stability, and durability of the films by the size and invariability of the loops. In addition, calculating diffusion coefficient values of ions that occur within the films from the CV graph also indicates the ability to color the films [29]. The diffusion coefficient value (Di) of ions generated within the films is according to Equation (3).

$$i_p = 2.72 \times 10^5 \times n^{2/3} \times Di^{1/2} \times C_0 \times v^{1/2} \quad (3)$$

where i_p is the maximum current, n is the number of electrons, C_0 is the concentration of active ions in the redox electrolyte, and v is the scan rate. The ion diffusion coefficient and area under the CV loop are shown in Tables 3-4 for quenching and cool-down conditions, respectively. The Cd-1.5 WO_3 showed the maximum diffusion coefficient value and has the biggest area under the loop with 3.535×10^{-7} $cm^2 \cdot s^{-1}$ and 3×10^{-5} AV, respectively. This calculation result is consistent with the morphology of the WO_3 films, which have a small grain size and are abundant, providing a large area for charge exchange within the films, according to Dahyun *et al.* [30]. The cool-down WO_3 films are more stable than quenching WO_3 due to their high crystallinity [28,31].

The optical properties of WO_3 films can be analyzed by their colored-bleached states. Figure 4 shows the transmittance of WO_3 films at wavelengths of 200 nm to1,000 nm. The cool-down WO_3 films were in the colored state, and the transmittance was lower than 10% in the wavelength range of 700 nm to 1,000 nm, less than the quenching WO_3 films. The average transmittance and the transmittance change were calculated by Equations (4) and (5), respectively, at 700 nm to 1,000 nm wavelengths between cool-down films and quenching films.

$$\%T_{av} = \frac{\sum_{\lambda_a}^{\lambda_b} T(\lambda)E(\lambda)}{\sum_{\lambda_a}^{\lambda_b} E(\lambda)} \quad (4)$$

$$\Delta\%T = \%T_{av_b} - \%T_{av_c} \quad (5)$$

where $\%T_{av}$ is the average transmittance, $T(\lambda)$ is the transmittance that depends on the wavelength, Relative energy is $\sum_{\lambda_a}^{\lambda_b} E(\lambda)$=100, $\%T_{av_b}$ is the average transmittance at the bleached state, and $\%T_{av_c}$ is the average transmittance at the colored state. The maximum transmittance changes for Q-0.5 and Cd-1.5 equal 26.75% and 48.20%, respectively. The results showed good consistency with the largest area in the CV loop.

WO_3 films obtained by improving the W films structure with annealing before anodization shows better structural properties and coloration efficiency compared with previous work [9]. Meanwhile, electrochromic properties under various conditions were compared with other research, as shown in Table 5. It was found that the WO_3 films prepared by anodization in this work showed relatively good electrochromic properties.

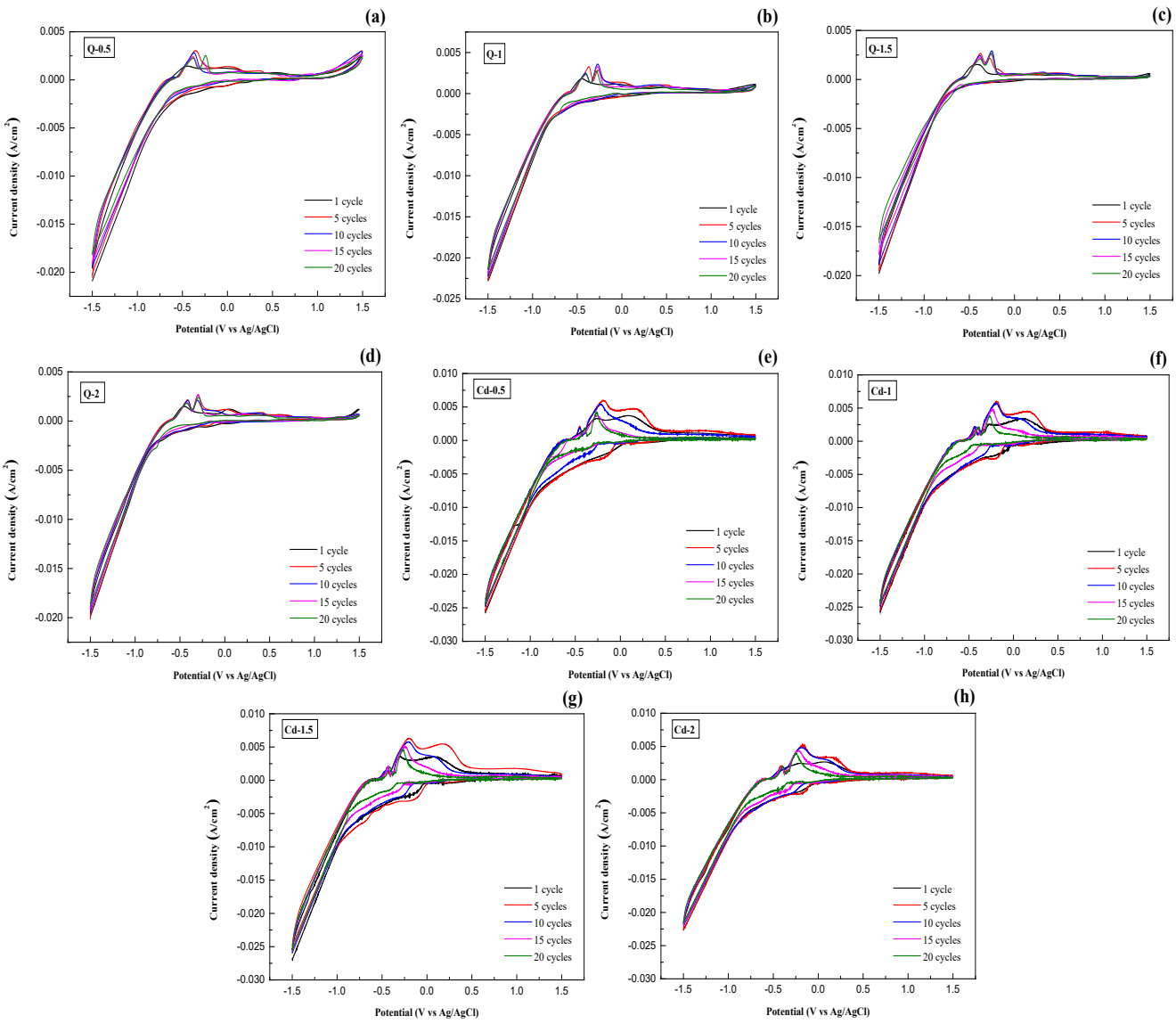

Figure 3. CV of WO_3 films of quenching (a-d), and cool-down (e-h) in 0.1 M H_2SO_4 solution with scan rate of 100 $mV \cdot s^{-1}$.

Table 3. The anodic/cathodic current peak and diffusion coefficient values of WO_3 films for quenching conditions.

Time (h)	Anodic peak current (10^{-3}) A·cm^{-2}	Anodic diffusion coefficient (10^{-7}) cm^2·s^{-1}	Cathodic peak current (10^{-3}) A·cm^{-2}	Cathodic diffusion coefficient (10^{-8}) cm^2·s^{-1}
0.5	5.956	4.795	2.116	6.052
1	5.918	4.734	2.423	7.935
1.5	6.283	5.336	2.532	8.665
2	5.132	3.56	2.066	5.769

Table 4. The anodic/cathodic current peak and diffusion coefficient values of WO_3 films for cool-down conditions.

Time (h)	Anodic peak current (10^{-3}) A·cm^{-2}	Anodic diffusion coefficient (10^{-7}) cm^2·s^{-1}	Cathodic peak current (10^{-3}) A·cm^{-2}	Cathodic diffusion coefficient (10^{-8}) cm^2·s^{-1}
0.5	3.036	1.246	1	1.352
1	3.250	1.428	0.851	0.979
1.5	2.639	0.941	0.407	0.224
2	2.602	0.915	0.439	0.26

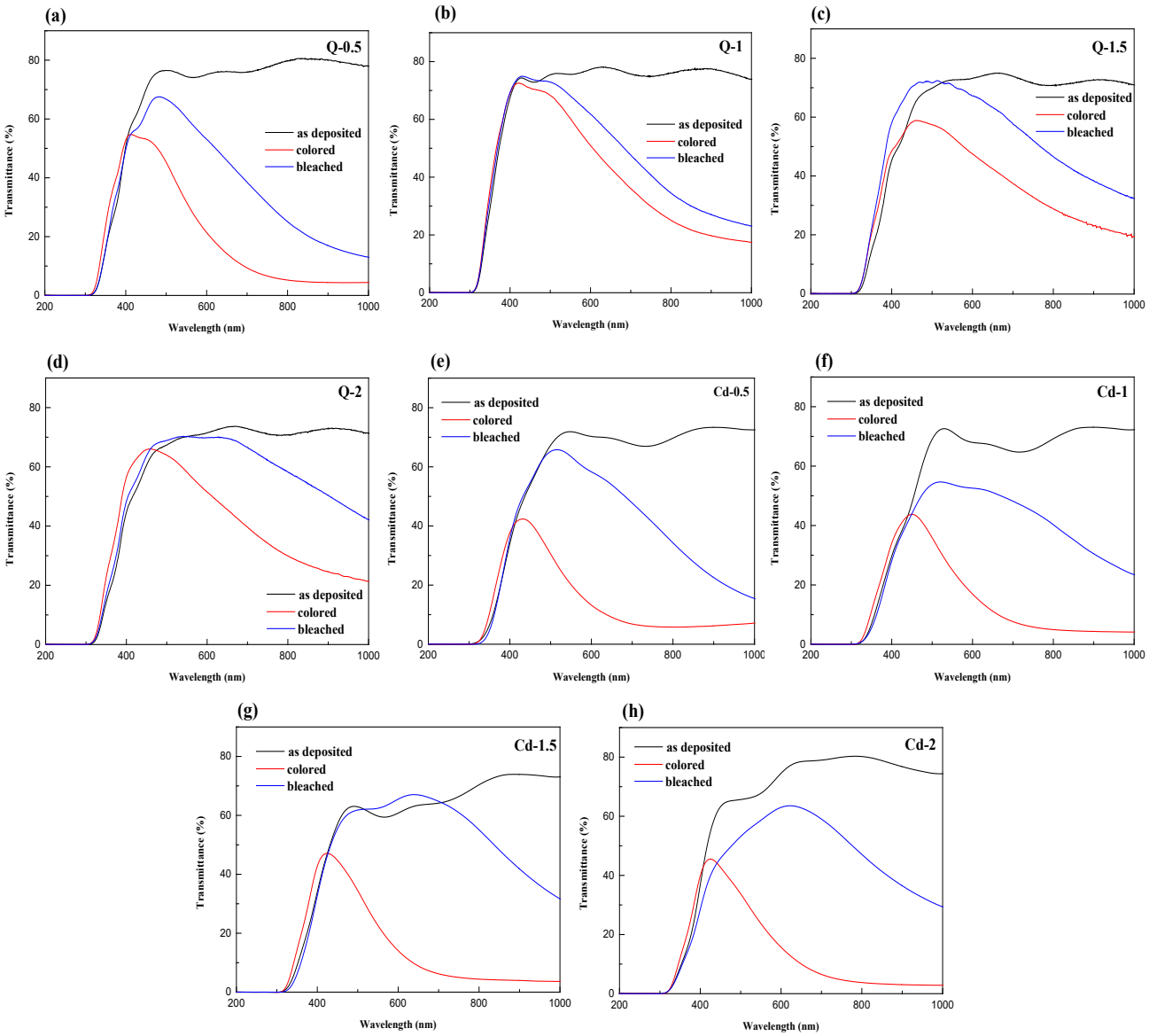

Figure 4. Transmission spectra of WO_3 films in the wavelength range of 200 nm to 1,000 nm of quenching (a-d), and cool-down (e-h).

Table 5. Comparison of the electrochromic performances of WO_3 films.

Method	Electrolyte	Δ%T (%)	Diffusion coefficient (Di) ($cm^2 \cdot s^{-1}$)	Reference
Kinetic spray technique	1 M $LiClO_4$	44	2.32×10^{-13}	[24]
Galvanostatic electrodeposition	1 M $LiClO_4$/PC	45.7	-	[32]
Electrodeposition	0.5 M $LiClO_4$/PC	89.81	2.04×10^{-10}	[33]
Anodization	0.1 M H_2SO_4	48.20	5.336×10^{-7}	This work

4. Conclusion

The W films were annealed at different times and treated with quenching and cool-down. After the anodization, WO_3 films exhibited different morphology, crystallinity, and electrochromic properties. The different treatment annealing times directly affected the morphology of WO_3. The morphology of WO_3 films for the cool-down condition showed a smaller grain size and was more porous than the quenching condition. These results enhanced the electrochromic properties of films with a maximum transmittance change of 48.20%. However, the film stability of the quenching condition showed better results than the cool-down condition. Improving films with good electrochromic properties and durability is an important future research issue.

Acknowledgments

This study was supported by Thammasat University Research Fund, Contract No TUFT 27/2567.

References

[1] C. Aiempanakit, A. Chanachai, N. Kanchal, M. Aiempanakit, and K. Aiempanakit, "Electrochromic property of tungsten trioxide films prepared by DC magnetron sputtering with oblique angle deposition and thermal oxidation," *Journal of Metals, Materials and Minerals*, vol. 31, pp. 123-128, 2021.

[2] D. Zhou, and L. Yang, "Enhanced electrochromic properties of nanocrystalline molybdenum oxide f ilms modified by dopamine," *Coatings*, vol. 13, pp. 1292, 2023.

[3] B. Zhang, C. Xu, G. Xu, S. Tan, and J. Zhang, "Amorphous titanium dioxide film with improved electrochromism in nearinfrared region," *Optical Materials*, vol. 89, pp. 191-219, 2019.

[4] W. Zhao, J.Wang, B. Tam, P. Pei, F. Li, A. Xie, and W. Cheng, "Macroporous vanadium oxide ion storage films enable fast switching speed and high cycling stability of electrochromic devices," *Applied Materials & Interfaces*, vol. 14, pp. 30021-30028, 2022.

[5] W. Thongjoon, I. Chuasontia, K. Aiempanakit, and C. Aiempanakit, "Morphology and electrochromic property of chemical bath deposited NiO films at different $NiSO_4$ concentration," *Journal of Metals, Materials and Minerals*, vol. 32, pp. 87-92, 2022.

[6] V. Madhavi, P. Kondaiah, O.M. Hussain, and S. Uthanna, "Structural, optical and electrochromic properties of RF magnetron sputtered WO_3 thin films," *Physica B*, vol. 454, pp. 141-147, 2014.

[7] X. Li, Z. Li, W. He, H. Chen, X. Tang, Y. Chen, and Y. Chen, "Enhanced electrochromic properties of nanostructured WO_3 film by combination of chemical and physical methods," *Coatings*, vol. 11, pp. 959, 2021.

[8] C. Y. Ng, K. A. Razak, and Z. Lockman, "Effect of annealing temperature on anodized nanoporous WO_3," *Journal Porous Mater*, vol. 22, pp. 537–544, 2015.

[9] C. Aiempanakita, R. Momkhunthoda, and K. Aiempanakit, "Electrochromism in nanoporous tungsten trioxide films prepared through anodization and thermal oxidation," *Integrated Ferroelectrics*, vol. 222, pp. 84-92, 2022.

[10] Y. Liu, N. Jiang, Y. Liu, D. Cui, C.F. Yu, H. Liu, and Z. Li, "Effect of laser power density on the electrochromic properties of WO_3 films obtained by pulsed laser deposition," *Ceramics International*, vol. 47, pp. 22416-22423, 2021

[11] Y. Shi, M. Sun, W. Chen, Y. Zhang, X. Shu, Y. Qin, X. Zhang, H. Shen, and Y. Wu, "Rational construction of porous amorphous WO_3 nanostructures with high electrochromic energy storage performance: Effect of temperature," *Journal of Non-Crystalline Solids*, vol. 549, p. 120337, 2020.

[12] J. Zhang, X. L. Wang, X. H. Xia, C. D. Gu, Z. J. Zhao, and J. P. Tu, "Enhanced electrochromic performance of macroporous WO_3 films formed by anodic oxidation of DC-sputtered tungsten layers," *Electrochimica Acta*, vol. 55, pp. 6953-6958, 2010.

[13] P. V. Ashrit, "Dry lithiation study of nanocrystalline, poly-crystalline and amorphous tungsten trioxide thin-film," *Thin Solid Films*, vol. 385, pp. 81-88, 2001.

[14] Y. Zhang, X. Liang, T. Jiang, H. Liu, Y. Fu, D. Zhang, and Z. Geng, "Amorphous/crystalline WO_3 dual phase laminated films: Fabrication, characterization and evaluation of their electrochromic performance for smart window applications," *Solar Energy Materials and Solar Cells*, vol. 244, p. 111820, 2022.

[15] K. K. Purushothaman, G. Muralidharan, and S. Vijayakumar, "Sol-Gel coated WO_3 thin films based complementary electro-chromic smart windows," *Materials Letters*, vol. 296, p. 129881, 2021

[16] R.M. Fernandez-Domene, G. Rosello-Marquez, R. Sanchez-Tovar, M. Cifre-Herrando, and J. GarcíaAnton, "Synthesis of WO_3 nanorods through anodization in the presence of citric acid: Formation mechanism, properties and photoelectrocatalytic performance," *Surface & Coatings Technology*, vol. 422, p. 127489, 2021.

[17] J. Zhang, X.L. Wang, X.H. Xia, C.D. Gu, Z.J. Zhao, J.P. Tu, "Enhanced electrochromic performance of macroporous WO_3 films formed by anodic oxidation of DC-sputtered tungsten layers," *Electrochimica Acta*, vol. 55, pp. 6953-6958, 2010.

[18] T. Zhang, M. Paulose, R. Neupane, L. A. Schaffer, D. B. Rana, J. Su, L. Guo, and O. K. Varghese, "Nanoporous WO_3 films synthesized by tuning anodization conditions for photoelectrochemical water oxidation," *Solar Energy Materials and Solar Cells*, vol. 209, p. 110472, 2020.

[19] B. W. Au, A. Tamang, D. Knipp, and K. Y. Chan, "Post-annealing effect on the electrochromic properties of WO_3 films," *Optical Materials*, vol. 108, pp. 110426, 2020

[20] K. Kalantar-zadeha, A. Z. Sadek, H. Zheng, V. Bansal, S. K. Bhargava, W. Wlodarski, J. Zhu, L. Yu, and Z. Hu, "Nanostructured WO_3 films using high temperature anodization," *Sensors and Actuators B*, vol. 142, pp. 230–235, 2009.

[21] F. A. Akgul, G. Akgul, N. Yildirim, H. E. Unalan, and R. Turan "Influence of thermal annealing on microstructural, morphological, optical properties and surface electronic structure of copper oxide thin films," *Materials Chemistry and Physics*, vol. 147, pp. 987-995, 2014.

[22] K. Pandurangarao, V. C. Babu, and V. R. Kumar, "Synthesis and characterization of Ti-WO_3 films for electrochromic applications," *Optical Materials*, vol. 136, p. 113381, 2023.

[23] P. J. Boruah, R. R. Khanikar, and H. Bailung, "Synthesis and characterization of oxygen vacancy induced narrow bandgap tungsten oxide (WO_{3-x}) nanoparticles by plasma discharge in liquid and its photocatalytic activity," *Plasma Chemistry and Plasma Processing*, vol. 40, pp. 1019-1036, 2020.

[24] H. Kim, D. Choi, K. Kim, W. Chu, D. Chun, and C. S. Lee, "Effect of particle size and amorphous phase on the electrochromic properties of kinetically deposited WO_3 films," *Solar Energy Materials and Solar Cells*, vol. 177, pp. 44-50, 2018.

[25] K. V. Madhuri, and M. B. Babu, "Influence of substrate temperature on growth and electrochromic properties of WO_3 thin films," *Optik*, vol. 174, pp. 470-480, 2018.

[26] C. Aiempanakit, M. Aiempanakit, W. Thongjoon, S. Pudwat, and K. Aiempanakit, "Characterization and electrochromic properties of multi-morphology NiO films prepared by CBD and DC Techniques," *Optik*, vol. 287, pp. 171131, 2023.

[27] H. Kim, D. Choi, K. Kim, W. Chu, D. Chun, and C. S. Lee, "Effect of particle size and amorphous phase on the electrochromic properties of kinetically deposited WO_3 films," *Solar Energy Materials and Solar Cells*, vol. 177, pp. 44-50, 2018.

[28] Y. Zhao, X. Zhang, X. Chen, W. Li, L. Wang, F. Ren, J. Zhao, F. Endres, and Y. Li, "Preparation of WO_3 films with controllable crystallinity for improved near-infrared electrochromic performances," *ACS Sustainable Chem. Eng*, vol. 8, pp. 11658-11666, 2020.

[29] K. K. Purushothaman, ans G. Muralidharan, "The effect of annealing temperature on the electrochromic properties of nanostructured NiO films," *Solar Energy Materials & Solar Cells*, vol. 93, pp. 1195-1201, 2009.

[30] D. Choi, M. Son, T. Im, S. Ahn, and C. S. Lee, "Microstructure control of NiO-based ion storage layer with various sized NiO particles to evaluate the electrochromic performance," *Materials Chemistry and Physics*, vol. 249, p. 123121, 2020.

[31] Z. Xia, H. Wan, Y. Su, P. Tang, M. Dai, H. Lin, Z. Zhang, and Q. Shi, "Enhanced electrochromic properties by improvement of crystallinity for sputtered WO_3 film," *Coatings*, vol. 10, p. 577, 2020.

[32] M. Arslan, Y.E. Firat, S.R. Tokgoz¨, and A. Peksoz, "Fast electrochromic response and high coloration efficiency of Al-doped WO_3 thin films for smart window applications," *Ceramics International*, vol. 47, pp. 32570-32578, 2021

[33] S. B. Patil, and S. B. Sadale, "Size-dependent electrochemical kinetics of nano-granular WO_3 thin films," *Solar Energy Materials and Solar Cells*, vol. 245, pp. 111849, 2022